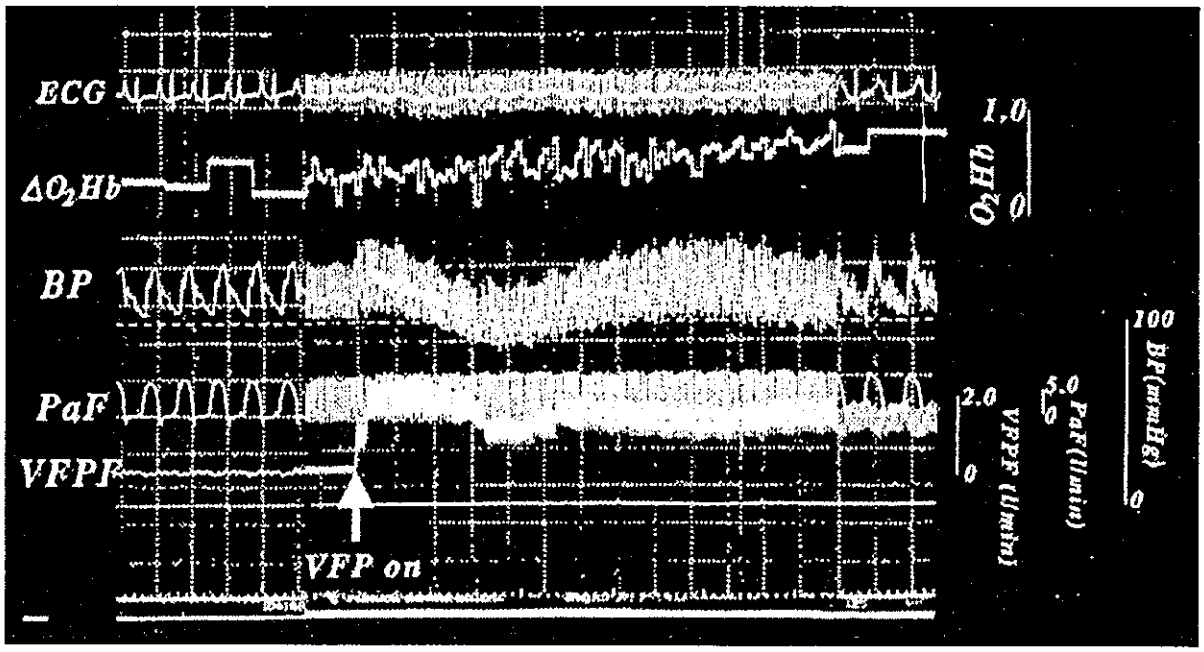

FIG. 2. Near-infrared spectroscopy during left ventricular assistance by VFP in an animal experiment. Increasing oxygenated hemoglobin (HbO_2) reflects cerebral blood flow changes. ECG, electrocardiogram; HbO_2, oxygenated hemoglobin; BP, arterial blood pressure; PaF, pulmonary artery flow; VFPF, vibrating flow pump flow.

hemodynamic parameters and HbO_2 using NIRO monitoring devices. With left heart assistance at 20–40%, the total flow (cardiac output) measured at the pulmonary arterial main trunk did not alter significantly. However, oscillating flow was recognized in the wave pattern of the pulmonary arterial wave. Oxygenated hemoglobin was measured using near-infrared spectroscopy. Measuring HbO_2 was possible using a NIRO monitoring system. An example is shown in a Fig. 2. Oscillating flow was added to the waveform at the start of the left heart assistance. Oscillating flow appears on the waveform at this time. At 20–40% of bypass, the total flow did not alter significantly. An increase in HbO_2 was observed after the induction of left heart assistance with the VFP.

To optimize the physiological 1/R (Abe et al.), control system, a circulatory control algorithm based on total peripheral vascular resistance was used in both our mock and animal experiments (4). Acute animal experiments using adult goats were performed. Centrifugal pumps were connected to the circulatory system of the goat with the inflow cannula of the left pump inserted into the left atrium and the outflow cannula sutured to the descending aorta while the inflow cannula of the right pump was inserted into the right atrium and the outflow cannula was sutured to the pulmonary artery. When blood circulation was stabilized, the natural heart was stopped by passing an electric current through the cardiac muscles. Total blood circulation was then maintained by the centrifugal pumps. Figure 3 shows the results of simultaneously applying 1/R control to the left pump and a left atrial pressure (LAP)-based control algorithm to the right pump. An increase in peripheral vascular resistance induced by injection of methoxamine hydrochloride at time $t = 3$ s initiated the response of maintaining blood pressure levels by reducing the left pump flow rate.

DISCUSSION

Through this experiment, the basic performance of the VFP as a VAD was confirmed. With oscillating blood flow, there is a risk of arrhythmia. However, significant arrhythmia due to vibration was not found in this case. The left heart assistance effect was sufficient to control for arrhythmia.

With a bypass ratio of 20–40%, the influence of vibration added to the waveform was examined. In this study, the total flow was altered. Accordingly, only the influence of high frequency waveforms was observed. As a result, an increase in the HbO_2 in the brain was observed. This experiment used anesthesia.

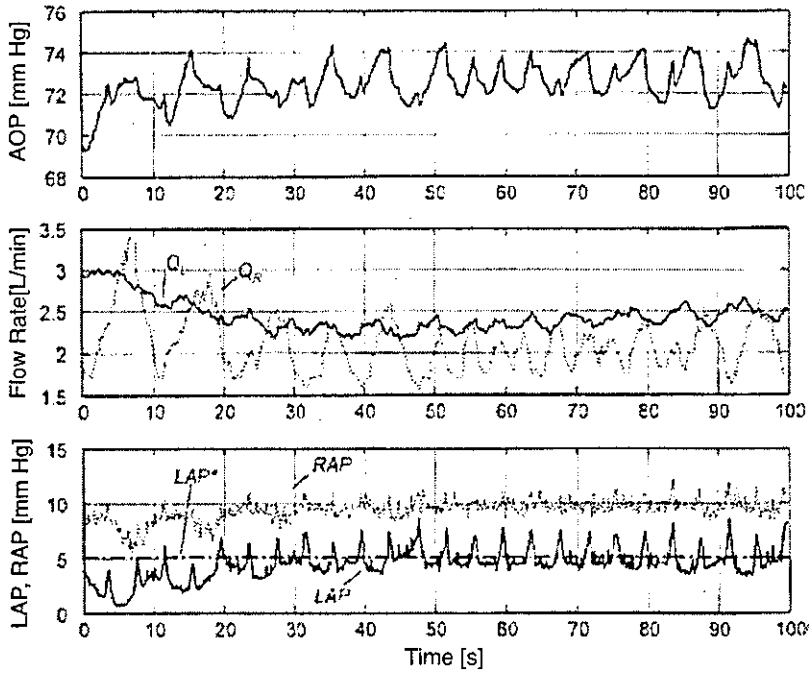

FIG. 3. The graph shows the results of an acute animal experiment when LAP-based right pump control is applied simultaneously with 1/R control. AOP, aortic pressure; Q_L, left pump flow rate; Q_R, right pump flow rate; LAP, left atrial pressure; RAP, right atrial pressure; LAP*, reference left atrial pressure.

Accordingly, the cerebral nerve function, being highly advanced was regarded as being in a fixed state. In other words, oxygen consumption was regarded as uniform. The HbO_2 increased during a constant state of brain function. This increase indicates an increase in brain blood flow. If brain blood flow increases during fixed oxygen consumption, the HbO_2 will increase accordingly.

In other words, only brain blood flow was thought to increase even though total blood flow was fixed. This phenomenon may be due to the waveform effect. This possibile effect of high frequency oscillating flow was noted. In addition, this phenomenon suggests a change in blood flow distribution. When the total blood flow was fixed, the artificial heart permitted an increase in brain blood flow. In addition to brain blood flow, the possibility that blood flow did decrease was discussed. In other words, blood flow distribution altered.

It has been reported that brain blood flow increases although the total flow of the circulation did not change when it was run at a frequency between 25 and 30 Hz. In other words, the distribution of organ perfusion changed. Additional experiments were performed to record the blood flow in other organs. Interestingly, renal blood flow increased at a frequency almost identical to that of VFP ventricular assistance. It is interesting that the brain and kidney may share frequency characteristics. Therefore, the most important and necessary parts may be protected, at least at the cost of the blood flow to other organs.

In the 1/R control system, since the left atrial pressure must be maintained within a relatively narrow range, it is recommended that right pump flow control have a quick response. However, since there is a connection between the right pump and left atrium, and the right pump flow rate may increase in the right atrium depending on the control parameters, it is necessary that the dynamic characteristics of pulmonary circulation be carefully considered when determining the control parameters for the right pump. As a safety measure, limits to the rate of increase in the right pump rotational speed may be introduced. In our proposed control algorithm, it is difficult to compensate for the sudden decrease in atrial pressure associated with this pulsatile motion. It is therefore necessary to introduce a method of estimating the amount of blood in the left atrium or to manipulate the right pump flow rate in advance to anticipate changes in the left pump flow rate (5,6).

We are also collaborating with the Imachi group to develop another compact undulation pump. The undulation pump total artificial heart (UPTAH) is a small implantable, completely artificial heart using two undulation pumps (7,8). It can produce arbitrary flow patterns: continuous flow, pulsatile flow based on continuous flow, and completely pulsatile flow, by

FIG. 4. Undulation pump total artificial heart.

changing the motor rotational speed of the UPTAH (Fig. 4). The left and right pumps are driven by pulsatile flow for generating cardiac output flow that is like the cardiac output flow of the natural heart. The size of the UPTAH is 76 mm in diameter and 78.5 mm in length. Its weight and volume are 620 g and 292 mL, respectively. The maximum output is about 11 L/min against 100 mm Hg pressure load when the motor speed is 1800 rpm. Two-month survival has been obtained with this unique implantable TAH using continuous flow displacement-type blood pumps. Therefore, this undulation pump is expected to be a preclinical, small, total artificial heart (TAH) with high performance.

Creating an artificial heart is not the final goal of our studies; in fact, we are aiming to develop artificial heart muscle. Artificial heart muscle would be sewn onto the ventricle to support the contraction power of the natural heart ventricle. Our artificial myocardium muscle supports the contraction of the natural heart ventricle; a compact, lightweight actuator using shape memory alloy (SMA) with a Peltier element actuator that may make a high-efficiency drive possible. The SMA actuator can be miniaturized.

For completly implantable blood pumps, we have developed a nanosensor that can measure biophysiological imformation in the body, especially for compact artificial hearts. The sensor is only 125 μm, and it can be attached to the surface of the heart and inserted into vessels using low invasive techniques (9,10).

CONCLUSION

The ability to control and monitor implanted medical assist devices has been successfully developed and demonstrated. Vibrating flow pumps can increase cerebral perfusion and alternate organ perfusion that can be used in drug delivery systems in the future. Optimization of the undulation pump total artificial heart design ofadvanced rotary blood pump is currently ongoing for preclinical use.

REFERENCES

1. Yambe T, Nitta S, Katahira Y, et al. Effect of left ventricular assistance on sympathetic tone. *Int J Artif Organs* 1990;October 13:681–6.
2. Nitta S, Hashimoto H, Sonobe T, et al. The newly designed univalved artificial heart. *ASAIO Trans* 1991;37:M240–1.
3. Kawano ST, Isoyama S, Kobayashi H, et al. Miniature vibrating flow blood pump using a cross-slider mechanism for external shunt catheter. *Artif Organs* 2003;27:73–7.
4. Abe Y, Chinzei T, Mabuchi K, et al. Over 500 days survival of a total artificial heart goat with 1/R control. In: Akutsu T, Koyanagi H, eds. *Heart Replacement: Artificial Heart 6*. Tokyo: Springer-Verlag, 1998;34–40.
5. Olegario PS, Yoshizawa M, Tanaka A, et al. Outflow control for avoiding atrial suction in a continuous flow total artificial heart. *Artif Organs* 2003;27:92–8.
6. Saito I, Chinzei T, Abe Y, et al. Progress in the control system of the undulation pump total artificial heart. *Artif Organs* 2003;27:27–33.
7. Abe Y, Chinzei T, Isoyama T, et al. One month survival with the undulation pump total artificial heart in a goat. *Artif Organs* 2001;25:69–71.
8. Abe Y, Chinzei T, Ono T, et al. Implantation of the undulation pump total artificial heart in the goat. *Artif Organs* 1999;23:932–8.
9. Yambe T, Kobayashi S, Yoshizawa M, et al. Recent progress on the vibrating flow pump as a totally implantable ventricular assist device. *Artif Organs* 2001;25:688–91.
10. Yambe T, Maruyama L, Takagi T, et al. Smallest ventricular assist system by use of Peltier elements with shape memory alloy. *Journal of Congestive Heart Failure and Circulatory Support* 2001;1:403–5.

Tohoku J. Exp. Med., 2004, **203**, 17-29

Beat-to-Beat Evaluation of Systolic Time Intervals during Bicycle Exercise Using Impedance Cardiography

TAKASHI ONO, MIHARU MIYAMURA, YOSHIFUMI YASUDA,[1] TOMONORI ITO,[1] TOSHIKAZU SAITO,[2] TOSHIMICHI ISHIGURO,[2] MAKOTO YOSHIZAWA[3] and TOMOYUKI YAMBE[4]

Research Center of Health, Physical Fitness and Sports, Nagoya University, Nagoya 464-8601,
[1]Health Science Center, Toyohashi University of Technology, Toyohashi, 441-8580,
[2]Chunichi-denshi Co. Ltd., Nagoya 458-8525,
[3]Information Synergy Center, and [4]Institute of Development, Aging and Cancer, Tohoku University, Sendai 980-8575

ONO, T., MIYAMURA, M., YASUDA, Y., ITO, T., SAITO, T., ISHIGURO, T., YOSHIZAWA, M. and YAMBE, T. *Beat-to-Beat Evaluation of Systolic Time Intervals during Bicycle Exercise Using Impedance Cardiography.* Tohoku J. Exp. Med., 2004, **203** (1), 17-29 —— In order to elucidate the beat-to-beat changes of the systolic time intervals (STI) during exercise, we proposed new techniques relating to an adaptive filter and detection algorithms for B- and X-points in the impedance cardiograph (ICG). Six male subjects underwent a ramp bicycle exercise up to maximum intensity during which an ECG, ICG and phonocardiogram (PCG) were continuously measured. Following the application of an adaptive filter, the scaled Fourier linear combiner (SFLC), to the first derivative (dZ/dt) of the base impedance (ΔZ) and PCG waveforms, the B- and X-points were automatically determined. For the B-point detection we used three criteria: the zero-crossing point (B_{zero}), the 15% response point ($B_{15\%}$) of the negative peak of the dZ/dt (dZ/dt_{min}) and a new algorithm (B_{new}). The X-point was separately determined by using the ICG and PCG waveforms. It was found that the shape of the dZ/dt waveform directly affected the determination of the B- and X-points. The B-points determined using B_{zero} and $B_{15\%}$ criteria were sometimes unstable caused by the location of a notch preceding the dZ/dt_{min} compared to the B_{new}. The time difference between the X-points measured by the ICG and PCG was mostly within ± 20 milliseconds but statistically significant. Although a wide variation was seen in R-R intervals, the STI were more stable. The relationships between HR and STI from rest to maximal exercise showed a gentle curvilinear relationship. It is suggested that the STI can be obtained precisely on a beat-to-beat basis by using the adaptive filter and detection algorithms for the inflection points of the ICG even during maximum exercise. ——— left ventricular ejection time; pre-ejection period; total systolic interval; impedance cardiography; ramp exercise

Received November 4, 2003; revision accepted for publication March 8, 2004.
Address for reprints: Yoshifumi Yasuda, Health Science Center, Toyohashi University of Technology, 1-1 Hibarigaoka, Tenpaku, Toyohashi 441-8580, Japan.
e-mail: yasuda@hse.tut.ac.jp

The systolic time intervals (STI): the left ventricular ejection time (LVET), pre-ejection period (PEP), total systolic interval (TSI) etc., had been used for the evaluation of the contractility of the myocardium, and/or the diagnosis of cardiovascular disorders. Previously, these parameters had been mainly determined by using the electrocardiogram (ECG), phonocardiogram (PCG) and carotid pulse tracing; however, carotid pulse tracing was often thought to be difficult due to movement artefacts, especially during exercise (Pigott and Spodick 1971; Wolfe et al. 1978). The impedance cardiograph (ICG) that was firstly proposed by Kubicek et al. (1966, 1970) for the measurement of stroke volume (SV) and cardiac output ($\dot{Q}$), had been also used for the measurement of LVET, PEP and other parameters relating to the cardiac cycle (Lababidi et al. 1970; Máttar et al. 1991). However, controversy remains on how to determine these parameters from the ICG. For example, Kubicek et al. (1966) had first introduced a method in determining the LVET from the zero-crossing or a deflection point just preceding the maximum negative peak (dZ/dt_{min}) of the dZ/dt waveform (B-point), to the positive peak of the dZ/dt waveform in the region of the second heart sounds (X-point). Thereafter, they revised the algorithm for the determination of B-point from the zero crossing point to the 15% response point of the dZ/dt_{min} (Kubicek et al. 1970). Although the reason for this modification has not been clarified yet, the latter criterion might be introduced to avoid misjudgements due to noise around the base line rather than physiological means. Furthermore, as mentioned by Kubicek et al. (1966), a small notch preceding the dZ/dt_{min} would be a lead for the B-point, but its detection might bring about many misjudgements (Fahrenberg et al. 1997). Sherwood et al. (1990) noted that the B-point might sometimes take the form of a subtle inflexion rather than appearing as a clear incisura. With reference to the above results, it may be summarized that the determination of the aortic valve opening by using the ICG is still obscure. With respect to the determination of the aortic valve closure, the nadir of the upward deflection (X-point) in the dZ/dt waveform has been used, but it is often ambiguous (Miles and Gotshall 1989; Sherwood et al. 1991). Miles and Gotshall (1989) recommended the usage of the PCG waveform in identifying the aortic valve closure when the X-point in the ICG is ambiguous, however, the synchronization between the X-points determined by ICG and PCG has not been systematically examined from rest to heavy exercise.

Moreover, the thoracic electrical impedance includes the signals derived not only by cardiovascular movements, but also by respiration, body movement, or other sources. These various origins of the impedance signals may bring about misjudgments for detecting B-, X- and/or other points. Several types of filters: a high pass filter and a band pass filter had been used for the elimination of noises outside of the known frequency band. However, the frequency band of respiration and body movements sometimes overlapped with the frequency band derived by cardiovascular events. Barros et al. (1995) proposed an adaptive filter that can selectively pass the frequency components synchronous with R-R interval in ECG. This technique may allow the elimination of noises and reduce inaccuracies of the inflection points in the dZ/dt waveform (Ono et al. 2004). In the present study, we firstly aimed, therefore, to examine the reliability for the determination of the so-called B- and X-points by different criteria by using an adaptive filter and detection algorithms on the dZ/dt waveform.

However, the changes of LVET and PEP against heart rate (HR) during exercise had been evaluated by different protocols such as carotid pulse tracing, echo ultrasound or ICG, showing an inverse linear relationship between them (Van der Hoeven et al. 1977; Miyamoto et al. 1983). These relationships were obtained only for a small number of subjects and/or small experimental situations, probably due to the methodological limitation. The technique noted above permits a continuous and beat-to-beat measurement of the

LVET, PEP, and TSI even during exercise. The second purpose of the present study was to evaluate the beat-to-beat relationships between LVET and HR, between PEP and HR, and between TSI and HR during a ramp bicycle exercise, from unloaded to maximal intensity on different subjects.

Materials and Methods

Subjects

After obtaining their informed consent, six healthy male students voluntarily participated in this study. Average values and standard deviations (±S.D.) of age, height and body weight were 20.5±1.4 years, 170.8±2.3 cm, and 62.8±6.1 kg, respectively. Each subject had been familiarized with all measurement devices and the experimental procedure before the study. The Human Subjects Review Committee at the Toyohashi University of Technology approved all experimental procedures.

Experimental procedure

The subjects underwent a ramp bicycle exercise up to a maximum intensity level using an automated electro-magnetic bicycle ergometer designed in our laboratory (Ito et al. 1996). The ergometer system consisted of a bicycle ergometer (Aerobike300, Combi, Tokyo), a photo-sensor, a torque meter, a power supply and a microcomputer. The power output of the ergometer was controlled by the PID feedback control theory with a frequency of 50 Hz. Following an unloaded pedalling on the ergometer for 2 minutes, the power output was automatically increased in a linear fashion by an incremental rate of 20 $W \cdot min^{-1}$.

During an unloaded and a ramp exercise, an electrocardiogram (ECG), a phonocardiogram (PCG) and an impedance cardiograph (ICG) were continuously measured. The ECG and PCG were obtained with a standard bipolar lead from the chest using a bioamplifier (AC-601G, Nihon Kohden, Tokyo) and a PCG unit (AS-601H, Nihon Kohden), respectively. The transthoracic impedance was also measured using a standard ICG unit (AI-601G, Nihon Kohden) with disposable spot electrodes. Four electrically connected spot electrodes were placed around the base of the neck and four electrodes placed around the thorax at the level of the xiphoid as the inner voltage electrodes. An upper current electrode was set at the central forehead and another lower current one at the lateral side of the lower ribcage. The impedance signals: basic thoracic impedance (Z_0) and its relative change (ΔZ), ECG and PCG were continuously recorded on a digital data recorder (MD-120TE, TEAC, Tokyo) at a sampling frequency of 200 Hz for subsequent analyses.

Data analyses

The dZ/dt signal was obtained from the first differentiation of the ΔZ, and then the adaptive filter, the scaled Fourier linear combiner (SFLC), was applied. The algorithm of the SFLC was based on the hypothesis that the required signal can be expressed as a sum of sine and cosine curves in a Fourier series in a period of T determined as each R-R interval in ECG. The basic algorithm of this filter had been previously reported by Barros et al. (1995).

In the ECG waveform, the positions of the onset of the Q wave, R spike, and the end of the T wave were determined by using a low pass filter and a peak detection algorithm. The HR was calculated from each R-R interval (RRI). For the detection of the B-point, we used three criteria. Firstly, the zero crossing point of the dZ/dt waveform just before the dZ/dt_{min} (B_{zero} indicated as ① in Fig. 1). Secondly, the 15% response point of the dZ/dt_{min} ($B_{15\%}$ indicated as ③ in Fig. 1) from the baseline, and thirdly, a new algorithm for the determination of the intersection between the zero-line and the regression line calculated from the 40% to 80% data of the descending curve of the dZ/dt_{min} (B_{new} indicated as ② in Fig. 1). The B_{new} algorithm was produced in order to search a notch located between zero and the dZ/dt_{min} in the waveform. The X-point was separately determined as the peak of the upward deflection of the dZ/dt waveform located around the end of T wave

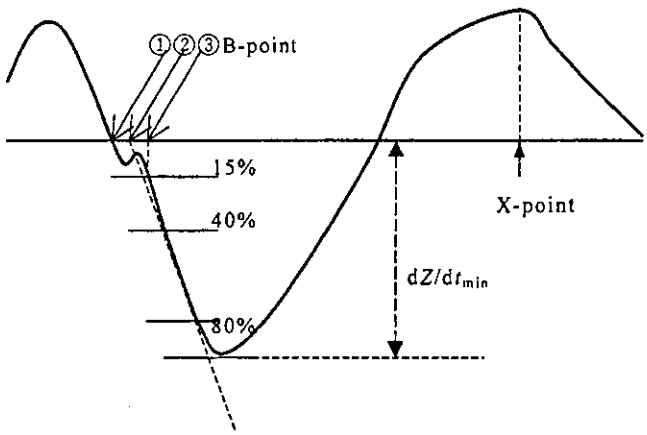

Fig. 1. Schematic presentation for the determination of the B-point using different criteria: 1) the zero crossing point of the dZ/dt waveform just before the dZ/dt_{min} (B_{zero}), 2) the 15% response point of the dZ/dt_{min} ($B_{15\%}$), and 3) a new algorithm for detecting the cross-point between the 0-line and the regression line which was calculated from the 40 to 80% response of the descending limb of the dZ/dt_{min} (B_{new}). The horizontal line shows the zero value of the dZ/dt.

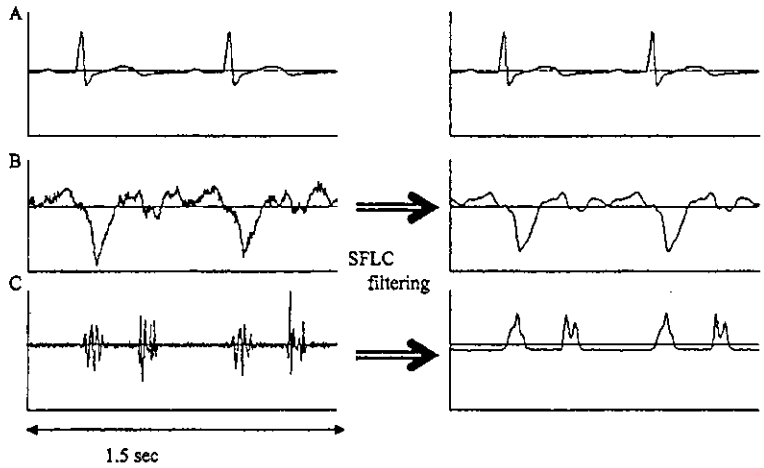

Fig. 2. A typical example of A: ECG, B: dZ/dt and C: PCG waveforms before and after the treatment of the SFLC. As shown in the figure, it seems in the filtered dZ/dt waveform that a small vibration and a slow wave around the base line could be mostly eliminated by the SFLC. Furthermore, the rectified and filtered PCG waveform could also be detected at the onset of the second heart sound.

(Lababidi et al. 1970) (X_{ICG}), and the onset of the second heart sound in the rectified and filtered PCG waveform (X_{PCG}). The time intervals from Q to B-point, from B- to X-points, and from Q to X-point were determined as the preejection period (PEP), left ventricular ejection time (LVET) and total systolic interval (TSI), respectively. Time resolution of each variable was every 5 milliseconds depending on a sampling frequency.

Statistical analysis

The beat-to-beat values of the STI, determined using different criteria, were compared with each other by means of the paired *t*-test and the Wilcoxon signed-ranks test. The statistical significance was set at 0.05. The relationships be-

tween HR and PEP, between HR and LVET, and between HR and TSI were fitted by a linear equation and an exponential equation using the least squares method. A coefficient of determination (r^2) was also calculated as the degree of conformity of the fitted curve.

Results

Fig. 2 shows a typical example of the data for ECG, dZ/dt and PCG waveforms with and without filter. As in the figure, it seems in the filtered dZ/dt waveform that small vibrations could be mostly eliminated and the inflection points could be clearly determined through filtering compared to the raw dZ/dt waveform. Moreover, the rectified and filtered PCG waveform also made it possible to ascertain the onset of the second heart sound more easily.

Fig. 3 indicates typical patterns of the dZ/dt waveform on the determination of the B-point. The patterns could be roughly divided into three by the appearance or location of a notch preceding the dZ/dt_{min}. In the left panel a clear notch did not appear from zero to the dZ/dt_{min}, and in this case, the B-points usually appeared in the order of B_{zero}, B_{new}, and $B_{15\%}$ (Pattern A). In the middle, the notch was located between the zero-line and the 15% response of the dZ/dt_{min}. In this case, the B-points were detected in the order of B_{zero}, B_{new}, and $B_{15\%}$ (Pattern B). In the right panel, the notch appeared below the 15% response of the dZ/dt_{min}. In this case, the B-point was generally detected in the order of B_{zero}, $B_{15\%}$ and B_{new} (Pattern C). The patterns of the dZ/dt waveform varied among subjects and the phase of exercise, but it came together in the form of pattern A during mild to heavy exercise because a clear notch tended to disappear in this period.

Time differences among PEP determined by different criteria for B-point are shown in Fig. 4. Data indicated the values of (PEP_{zero}–PEP_{new}) and ($PEP_{15\%}$–PEP_{new}). The differences in ($PEP_{15\%}$–PEP_{new}) were almost within ± 5 milliseconds in four subjects (HA, OO, YA and YO), but were much more varied in two subjects (OH and TN). These differences between $PEP_{15\%}$ and PEP_{new} were significant ($p<0.001$) in all subjects. The changes in (PEP_{zero}–PEP_{new}) were generally larger than those in ($PEP_{15\%}$–PEP_{new}), and significant differences were seen between $PEP_{15\%}$ and PEP_{new} in all subjects.

Fig. 5 shows the differences between the TSI_{ICG} calculated from Q to X_{ICG} and the TSI_{PCG} from Q to X_{PCG} in each subject. The differences between TSI_{ICG} and TSI_{PCG} were varied among subjects: the mean values of TSI_{ICG} were significantly shorter than those of TSI_{PCG} in five of six subjects, but longer in one subject.

Time courses of the changes in RRI, TSI estimated from Q to X_{ICG}, LVET measured from B_{new} to X_{ICG}, and PEP_{new} from a sitting rest for 30 seconds to unloaded exercise for 2 minutes and followed by a ramp exercise on six subjects, are illustrated in Fig. 6. All these parameters

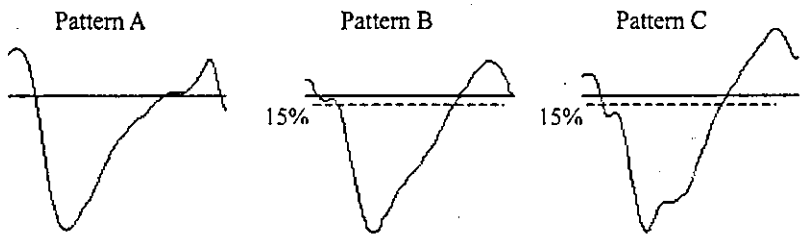

Fig. 3. The typical examples of the dZ/dt waveform according to the appearance of a small notch preceded the dZ/dt_{min}. The pattern was roughly divided into three: Pattern A indicates the case in which no clear notch was found (left panel), Pattern B indicates the case in which the notch was located between the base-line and the 15% response of the dZ/dt_{min} (middle panel), and Pattern C indicates the case in which the notch appeared below the 15% response of the dZ/dt_{min} (right panel).

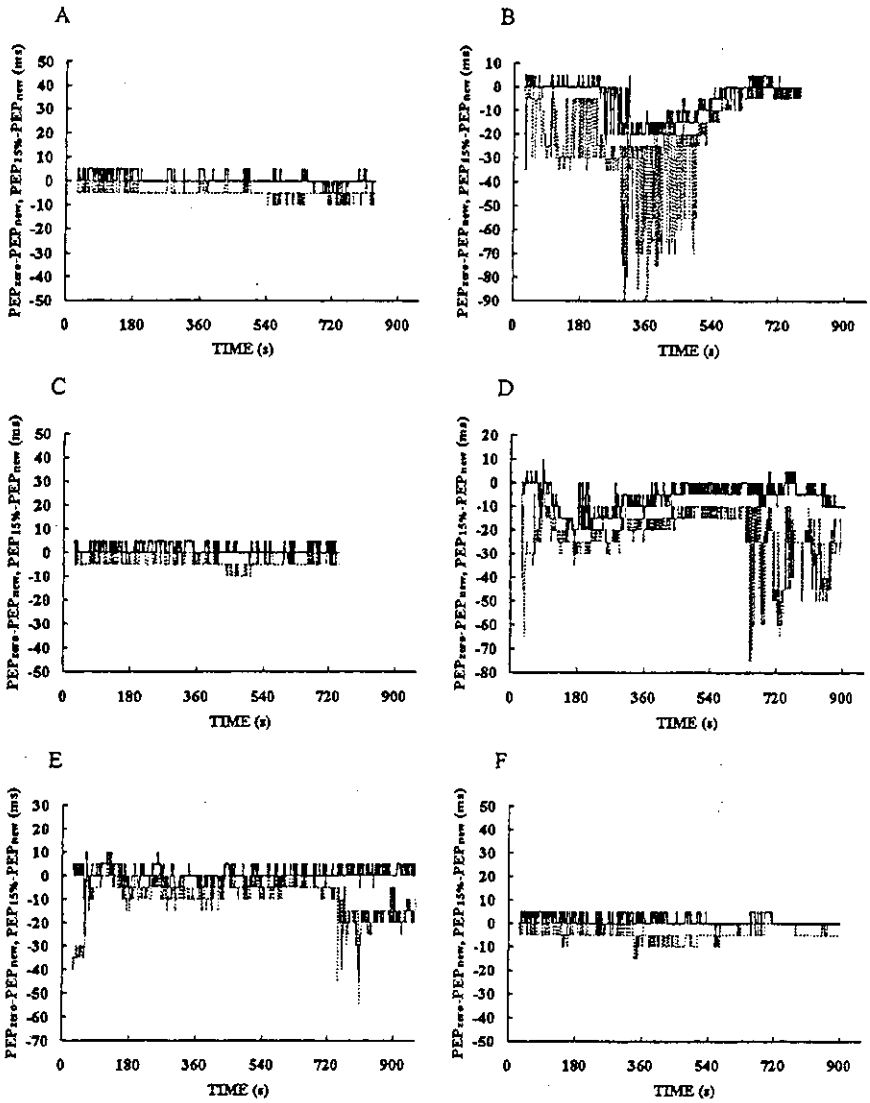

Fig. 4. Time courses of the PEP measured using different criteria on the six subjects. Data indicates the difference between PEP_{zero} to PEP_{new} (a solid line) and between $PEP_{15\%}$ and PEP_{new} (a dotted line). The mean values and ±S.D. of the (PEP_{zero}–PEP_{new}) and the ($PEP_{15\%}$–PEP_{new}) in each subject are as follows. A: Subj. HA, PEP_{zero}–PEP_{new}: −4.94±2.46 milliseconds, $p<0.001$, and $PEP_{15\%}$–PEP_{new}: 0.50 ±2.26 milliseconds, $p<0.001$. B: Subj. OH, PEP_{zero}–PEP_{new}: −17.62±18.14 milliseconds, $p<0.001$, and $PEP_{15\%}$–PEP_{new}: −4.56±7.71 milliseconds, $p<0.001$. C: Subj. OO, PEP_{zero}–PEP_{new}: −3.54± 2.93 milliseconds, $p<0.001$, and $PEP_{15\%}$–PEP_{new}: 1.26±2.20 milliseconds, $p<0.001$. D: Subj. TN, PEP_{zero}–PEP_{new}: −22.46±11.69 milliseconds, $p<0.001$, and $PEP_{15\%}$–PEP_{new}: −5.49±5.59 milliseconds, $p<0.001$. E: Subj. YA, PEP_{zero}–PEP_{new}: −9.92±7.76 milliseconds, $p<0.001$, and $PEP_{15\%}$–PEP_{new}: 0.84 ±3.13 milliseconds, $p<0.001$. F: Subj. YO, PEP_{zero}–PEP_{new}: −4.00±3.13 milliseconds, $p<0.001$, and $PEP_{15\%}$–PEP_{new}: 1.14±2.14 milliseconds, $p<0.001$. All these differences are statistically significant both by the paired t-test and the Wilcoxon signed-ranks test.

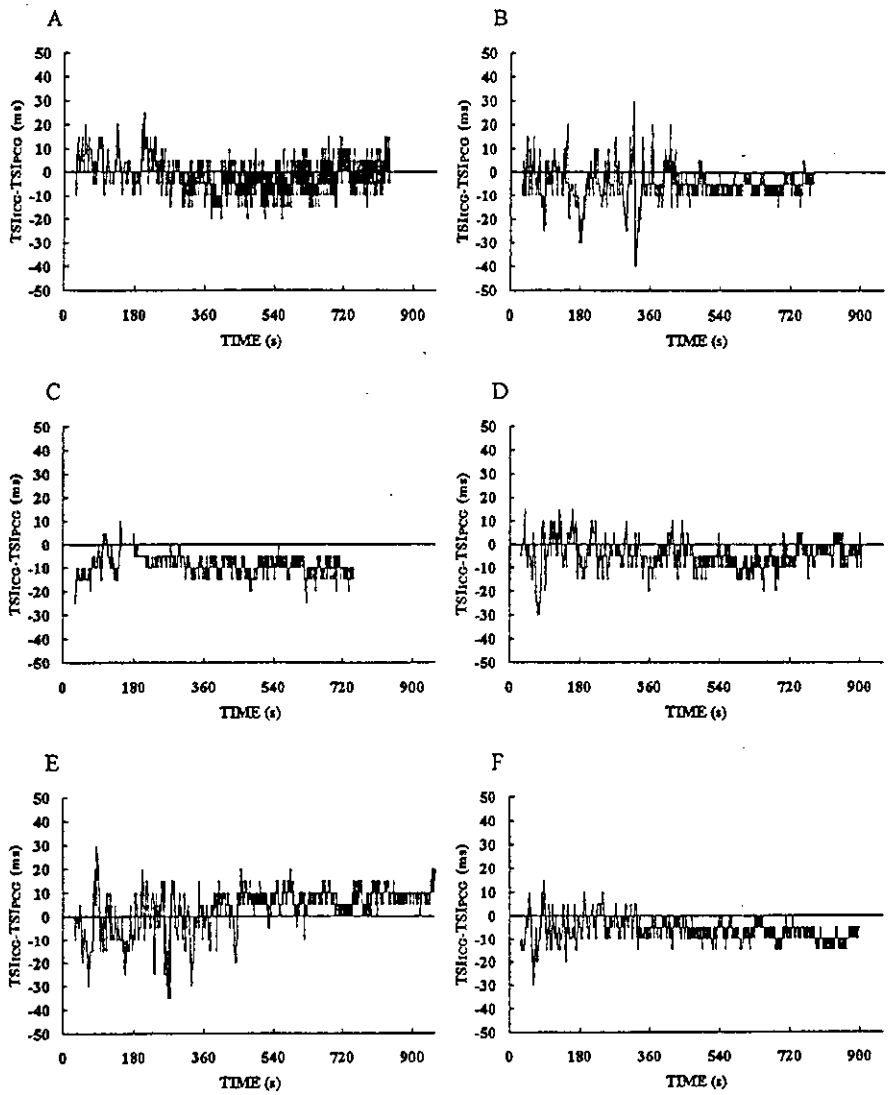

Fig. 5. Beat-to-beat differences between the total systolic intervals detected by ICG (TSI_{ICG}) and by PCG (TSI_{PCG}) from rest to maximal exercise in each subject. The mean value and ±S.D. in each subject are as follows. A: Subj. HA, TSI_{ICG}–TSI_{PCG}: −1.54±6.88 milliseconds, $p<0.001$. B: Subj. OH, TSI_{ICG}–TSI_{PCG}: −4.92±7.26 milliseconds, $p<0.001$. C: Subj. OO, TSI_{ICG}–TSI_{PCG}: −8.90±4.51 milliseconds, $p<0.001$. D: Subj. TN, TSI_{ICG}–TSI_{PCG}: −4.44±6.18 milliseconds, $p<0.001$. E: Subj. YA, TSI_{ICG}–TSI_{PCG}: 4.81±8.77 milliseconds, $p<0.001$. F: Subj. YO, TSI_{ICG}–TSI_{PCG}: −6.47±4.92 milliseconds, $p<0.001$. All these differences are statistically significant both by the paired t-test and the Wilcoxon signed-ranks test.

gradually decreased according to the increase of exercise intensity. The RRI seemed to fluctuate largely, from rest to light intensity of exercise, but it dropped under moderate and strenuous exercise. The pattern of changes in the TSI and LVET were quite similar to each other, but the pattern of the PEP clearly differed from those in the TSI and LVET.

Fig. 7 illustrates the beat-to-beat changes of the TSI, LVET, and PEP against the changes of HR and the fitted curves using an exponential equation among them. All data are the same as

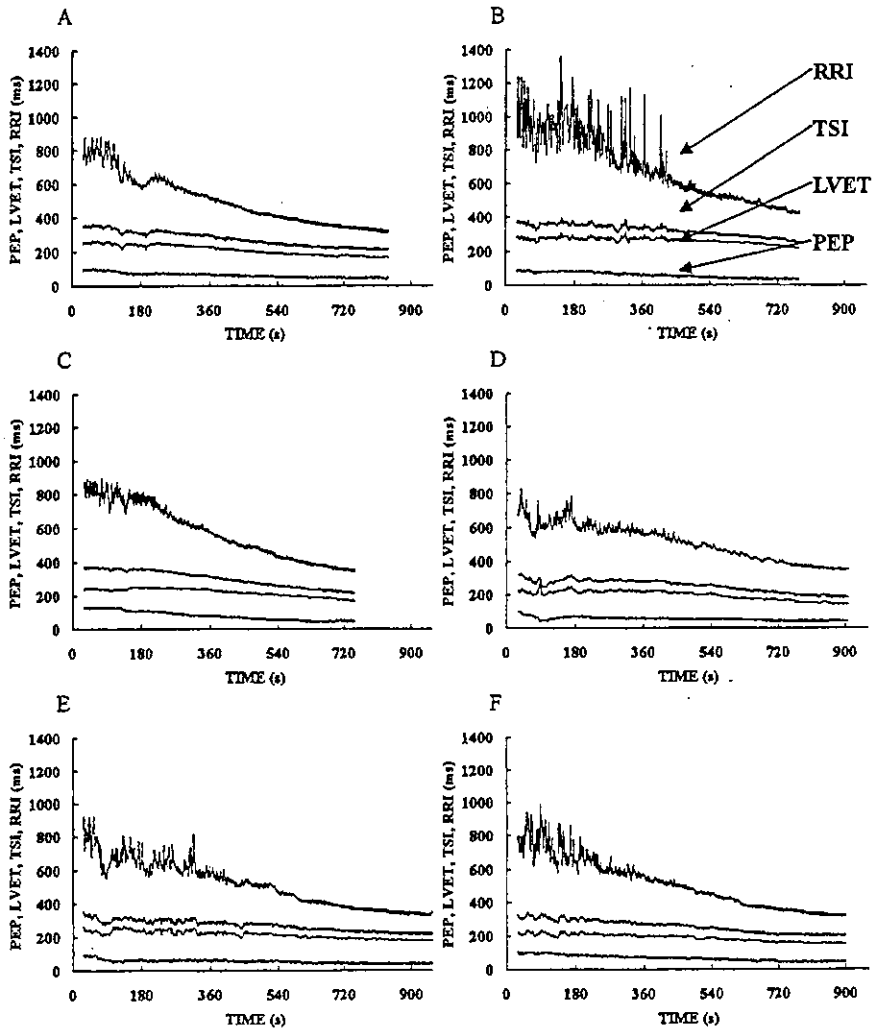

Fig. 6. The time courses of the RRI, TSI, LVET and PEP from rest for 30 seconds and 2 minutes unloaded exercise followed by a ramp exercise to maximum intensity in the six subjects (A: Subj. HA, B: Subj. OH, C: Subj. OO, D: Subj. TN, E: Subj. YA, and F: Subj. YO).

in Fig. 6. The mean values of the coefficient of determination (r^2) regressed by an exponential equation between HR and TSI, between HR and LVET and between HR and PEP were 0.966, 0.914 and 0.858; these were higher than those regressed by a linear equation: 0.963, 0.912 and 0.839, respectively. However, a significant difference was not observed between them. Furthermore, a wide variation was observed between HR and STI especially in the lower range of the HR.

Discussion

To our knowledge there are few studies that show the beat-to-beat changes of the STI (such as the LVET and PEP), with respect to the changes of HR (from rest to maximal intensity), during ramp exercise. Perhaps this is due to methodological difficulties. In the present study, we demonstrated the beat-to-beat changes of the STI from rest to maximal exercise by using an adaptive filtering technique and algorithms for the B-

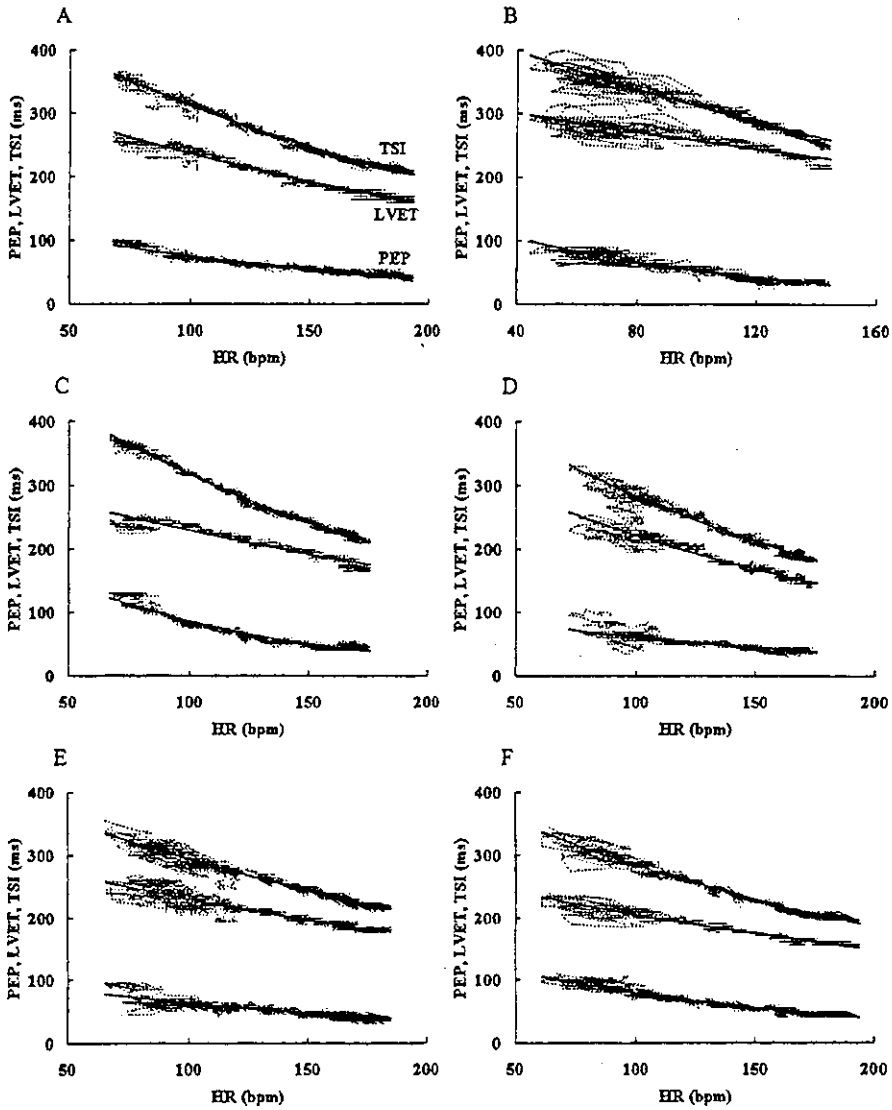

Fig. 7. The changes of the PEP, LVET and TSI against HR from rest to maximal exercise. The exponential equations and the coefficients of determination of the fitted curve in each subject are as follows. A: Subj. HA, PEP: $y=141.3e^{-0.0063x}$, $r^2=0.911$, LVET: $y=356.8e^{-0.0041x}$, $r^2=0.963$, TSI: $y=494.9e^{-0.0046x}$, $r^2=0.984$. B: Subj. OH, PEP: $y=165.3e^{-0.0114x}$, $r^2=0.877$, LVET: $y=332.9e^{-0.0026x}$, $r^2=0.788$, TSI: $y=470.4e^{-0.0046x}$, $r^2=0.935$. C: Subj. OO, PEP: $y=253.2e^{-0.0108x}$, $r^2=0.939$, LVET: $y=326.7e^{-0.0035x}$, $r^2=0.927$, TSI: $y=543.6e^{-0.0054x}$, $r^2=0.991$. D: Subj. TN, PEP: $y=114.5e^{-0.0063x}$, $r^2=0.727$, LVET: $y=385.3e^{-0.0055x}$, $r^2=0.936$, TSI: $y=501.5e^{-0.0057x}$, $r^2=0.957$. E: Subj. YA, PEP: $y=113.2e^{-0.0058x}$, $r^2=0.772$, LVET: $y=316.1e^{-0.0032x}$, $r^2=0.905$, TSI: $y=426.1e^{-0.0037x}$, $r^2=0.954$. F: Subj. YO, PEP: $y=162.8e^{-0.0072x}$, $r^2=0.924$, LVET: $y=285.3e^{-0.0033x}$, $r^2=0.952$, TSI: $y=437.4e^{-0.0043x}$, $r^2=0.975$.

and X-points detection in the dZ/dt waveform, and eventually clarified a gentle curvilinear relationship between HR and STI.

Filtering performance

As shown in Fig. 2, the raw dZ/dt waveform is noisy and it is often difficult to detect the inflection points of the waveform especially during exercise. In the present study, we used an adaptive filter, a scaled Fourier linear combiner (SFLC) to eliminate the noises (Barros et al. 1995; Ono et al. 2004). This filter was designed to eliminate noises asynchronous with the frequency of R-R interval. It was found, that by using the SFLC, the waveform of the dZ/dt became clear and the inflection points of the waveform could be determined more easily and precisely. Furthermore, the application of this technique also made it possible to determine the onset of the second heart sound in PCG more easily. It suggests from the above results that the SFLC must be a superior tool for the elimination of noises and thereby for the determination of the deflection points in the dZ/dt and PCG waveforms.

Validity for the determination of B- and X-points from the dZ/dt waveform

When evaluating the STI from ICG waveform, controversy remains especially on how to determine the B-point in the ICG. Kubicek et al. (1966) first introduced the determination of the B-point, which corresponded to the opening of the aortic valve, as the crossing point of the dZ/dt waveform with the base line (B_{zero}). Thereafter, they revised this criterion to the 15% response point ($B_{15\%}$) of the negative peak of the dZ/dt waveform (dZ/dt_{min}) from the baseline instead of the B_{zero}, probably in order to avoid any misinterpretations from the noises around the base line (Kubicek et al. 1970). Up to now, most of the studies attempting to determine the B-point by ICG have been via the B_{zero} method, and little research has been conducted employing the $B_{15\%}$ method (Miyamoto et al. 1981, 1988). Alternatively, Kubicek et al. (1966) noticed in their first study that a small notch preceding the dZ/dt_{min} would be the true B-point. However, this small notch might be ambiguous or disappear in the dZ/dt waveform especially during exercise (Sherwood et al. 1990; Fahrenberg et al. 1997). Wang et al. (1995) proposed the time-frequency distribution technique to determine the B- and X-points which involved finding a peak or inflexion point of the waveform, but this technique was not widely accepted because of the methodological difficulties. Due to the above reasons, the criterion for the detection of the notch might not be used for the measurement of the B-point. In the present study, we have proposed a new algorithm whose purpose is to detect a notch by using an extrapolation technique on the downslope of the dZ/dt_{min} from 40 to 80%. We firstly attempted to examine the effect of different criteria: B_{zero}, $B_{15\%}$ and B_{new} methods on the determination of PEP and relating problems.

Present results showed that the order of appearance of each B-point, detected by different criteria, varied depending on the shape of the dZ/dt waveform, and the appearance of each B-point could be divided into three typical patterns as illustrated in Fig. 3. In pattern A, each B-point appeared closely and the time differences were almost within ± 5 milliseconds (Subjects HA, OO and YO). In pattern B, the $B_{15\%}$ and B_{new} appeared closely as in the pattern A, but the B_{zero} sometimes differed largely from the other ones as observed in the subjects TN, YA and OH. In these subjects, the B_{zero} sometimes appeared preceding the Q-wave, and this might be unreasonable if one takes into consideration the physiological mechanism of the aortic valve opening, followed by the depolarization of the left ventricle. In pattern C, which was observed in subjects TN and OH, large differences ranging from 10 to 20 milliseconds were often observed between $B_{15\%}$ and B_{new}. From the above results it can be summarized that the conventional methods often provided unstable data due to the appearance or location of a notch, but the new method proposed here could provide more stable data as opposed to the conventional

methods. This is also proved indirectly by the smooth change of the PEP during exercise as shown in Fig. 6. However, in this present study, we were unable to identify the location of the true B-point that coincided with the aortic valve opening because we did not directly measure the aortic valve movement. Furthermore, we used the linear extrapolation technique on the data from the 40 to 80% response of the dZ/dt_{min} based on the hypothesis that dZ/dt waveform changed approximately in a linear fashion for this portion as in Fig. 1, and the notch did not exceed the 40% response of the dZ/dt_{min}. However, we could see a few exceptions in the results because the descending limb of the dZ/dt_{min} from 40 to 80% did show a curvilinear change rather than a linear fashion. Further improvements, therefore, should be required for a more accurate and valid determination of the B-point in the ICG.

Previous studies have shown that the X-point corresponding to the closure of the aortic valve was accredited the maximum positive peak of the dZ/dt waveform following the dZ/dt_{min} (X_{ICG}). This coincides with the onset of the second heart sound in PCG (X_{PCG}) (Kubicek et al. 1970; Lababidi et al. 1970; Miles and Gotshall 1989; Ono et al. 2004). However, the coincidence between X_{ICG} and X_{PCG} has not been investigated, especially during exercise, because PCG waveform is also noisy and often ambiguous when identifying the X_{PCG} similar to that in the dZ/dt waveform. In the present study, we applied the same filtering technique on the rectified PCG waveform and, because of this, the X_{PCG} could be detected more clearly (Fig. 2). As in Fig. 6, the time differences between TSI, measured by the X_{ICG} and X_{PCG}, were mostly within ± 20 milliseconds, but a significant difference was found in all subjects. In the five subjects: OH, OO, TN, HA and YO, the appearance of the X_{ICG} was significantly faster than that of X_{PCG}, and in contrast to this, the X_{ICG} was significantly delayed compared to the X_{PCG} in the subject YA. Although the real reasons for this discrepancy cannot be resolved here, some possible reasons can be put forward. Firstly, the misjudgment of the X_{ICG} may be of concern because the dZ/dt waveform corresponding to the end of T-wave in the ECG sometimes showed a near plateau or made double peaks rather than making a clear peak. In these cases, inaccuracies might have occurred. Secondly, previous studies that showed a good agreement between X_{ICG} and X_{PCG}, had measured the X-points only for a few beats and only at rest (Lababidi et al. 1970; Miles and Gotshall 1989). The present study here demonstrated that the difference between TSI_{ICG} and TSI_{PCG} fluctuated greatly at rest and during low-intensity exercise, but it was inhibited during mild to heavy exercise. It suggests, therefore, that the exercise intensity may modulate the appearance of the X-point. Further experiments will need to be conducted in order to resolve this problem.

Time courses of RRI, TSI, LVET and PEP from unloaded to ramp exercise

It has been well demonstrated that the time course of RRI during ramp exercise shows a curvilinear relationship with the increase of work rate or work time. As shown in Fig. 6, the present results also confirmed a curvilinear relationship between RRI and work time. The time courses of the TSI and LVET were similar to each other, but the fluctuation in each variable was much attenuated compared to that in RRI. The PEP seemed to be stable and did not show clear fluctuations.

Relationships HR versus TSI, PEP and LVET

A number of studies using different apparatuses including ICG, carotid pulse tracing or echo ultrasound, reported an inverse relationship between HR and STI mainly between HR and LVET (Van der Hoeven et al. 1977; Vanfraechem 1979; Miyamoto et al. 1983; Máttar et al. 1991). However, those relationships were measured only for several degrees of exercise intensity. In the present study, we demonstrated the beat-to-beat relationship between HR and STI from rest to maximal intensity during a ramp exercise, and observed a gentle curvilinear relationship between them. Therefore, an exponential equa-

tion was used to describe the relationship between HR and STI, but insignificant differences in the coefficients of determination (r^2) between the exponential and linear equations were observed. Therefore, the results obtained by the present study and the previous ones are thought to be essentially similar.

It has been clarified that the relationship between HR and TSI, obtained both at rest and during exercise, are modulated by several factors. These include body posture (Miyamoto et al. 1983; Smith et al. 1989), physical training (Vanhees et al. 1984; Krzemiński et al. 1989), aging and cardiovascular diseases (Van der Hoeven et al. 1977; Máttar et al. 1991; Thomas and Crowther 1993). For example, Miyamoto et al. (1983) reported that the regression line between HR and LVET shifted downward, but the regression line between HR and PEP was shifted upward by the postural change from supine to upright. Krzemiński et al. (1989) noted that endurance training shifted the HR-LVET relationship downward. Van der Hoeven et al. (1977) reported a significant change between HR and STI in patients with coronary insufficiencies compared to healthy individuals. Since it is possible to provide the beat-to-beat changes of the STI and HR, not only at rest but also during heavy exercise, the techniques proposed in the present study may have strong advantages for the evaluation of cardiovascular fitness or the diagnosis of cardiovascular dysfunctions.

Conclusion

In conclusion, it became possible to measure the STI on a beat-to-beat basis, not only at rest but also during heavy exercise. This was carried out by using an adaptive filtering technique and detection algorithms for the inflection points of the dZ/dt waveform in an ICG. The present technique may contribute to detailed and precise analyses of the relationships between HR and STI being modulated by aging, endurance training, and the degree of cardiovascular disorders.

References

Barros, A.K., Yoshizawa, M. & Yasuda, Y. (1995) Filtering noncorrelated noise in impedance cardiography. *IEEE Trans. Biomed. Eng.*, **42**, 324-327.

Fahrenberg, J., Forester, F. & Müller, W. (1997) Noninvasive estimations of ventricular ejection time and stroke volume: comparison of impedance cardiography and the Portapres 2. *J. Med. Eng. Technol.*, **21**, 15-22.

Ito, H., Ono, T., Yasuda, Y., Nishioka, M. & Horiuchi, O. (1996) Assessment for the equivalent inertia and energy transfer loss of the electro-magnetic bicycle ergometer. *Jpn. J. Sports Sci.*, **15**, 127-133. (in Japanese with English abstract)

Krzemiński, K., Niewiadomski, W. & Nazar, K. (1989) Dynamics of changes in the cardiovascular response to submaximal exercise during low-intensity endurance training with particular reference to the systolic time intervals. *Eur. J. Appl. Physiol.*, **59**, 377-384.

Kubicek, W.G., Karnegis, J.N., Patterson, R.P., Witsoe, D.A. & Mattson, R.H. (1966) Development and evaluation of an impedance cardiac output system. *Aerospace Med.*, **37**, 1208-1212.

Kubicek, W.G., Patterson, R.P. & Witsoe, D.A. (1970) Impedance cardiography as a noninvasive method of monitoring cardiac function and other parameters of cardiovascular system. *Ann. N. Y. Acad. Sci.*, **170**, 724-732.

Lababidi, Z., Ehmke, D.A., Durnin, R.E., Leaverton, P.E. & Lauer, R.M. (1970) The first derivative thoracic impedance cardiogram. *Circulation*, **41**, 651-658.

Máttar, J.A., Shoemaker, W.C., Diament, D., Lomar, A., Lopes, A.C., Freitas, E.D., Stella, F.P. & Factore, L.A.P. (1991) Systolic and diastolic time intervals in the critically ill patient. *Crit. Care Med.*, **19**, 1382-1386.

Miles, D.S. & Gotshall, R.W. (1989) Impedance cardiography: noninvasive assessment of human central hemodynamics at rest and during exercise. *Exerc. Sport Sci. Rev.*, **17**, 231-263.

Miyamoto, Y., Takahashi, M., Tamura, T., Nakamura, T., Hiura, T. & Mikami, M. (1981) Continuous determination of cardiac output during exercise by the use of impedance plethysmography. *Med. Biol. Eng. Comput.*, **19**, 638-644.

Miyamoto, Y., Higuchi, J., Abe, Y., Hiura, T., Nakazono, Y. & Mikami, T. (1983) Dynamics of cardiac output and systolic time intervals in supine and upright exercise. *J. Appl. Physiol.*,

55, 1674-1681.

Miyamoto, Y., Kawahara, K., Nakazono, Y., Grucza, R., Sugawara, T. & Sato, K. (1988) The origin of the initial abrupt increase in ventilation at the onset of muscular exercise (phase 1) in man. *Tohoku J. Exp. Med.*, **156**, Suppl., 113-123.

Ono, T., Yasuda, Y., Ito, T., Barros, A.K., Ishida, K., Miyamura, M., Yoshizawa, M. & Yambe, T. (2004) Validity of the adaptive filter for accurate measurement of cardiac output in impedance cardiography. *Tohoku J. Exp. Med.*, **202**, 181-191.

Pigott, V.M. & Spodick, D.H. (1971) Effects of normal breathing and expiratory apnea on duration of the phases of cardiac systole. *Am. Heart J.*, **82**, 786-793.

Sherwood, A., Allen, M.T., Fahrenberg, J., Kelsey, R.M., Lovallo, W.R. & van Doornen, L.J.P. (1990) Methodological guidelines for impedance cardiography. *Psychophysiology*, **27**, 1-23.

Smith, J.J., Muzi, M., Barney, J.A., Ceschi, J., Hayers, J. & Ebert, J. (1989) Impedance-derived cardiac indices in supine and upright exercise. *Ann. Biomed. Eng.*, **17**, 507-515.

Thomas, S.H.L. & Crowther, A. (1993) Impedance cardiography during exercise in patients with coronary heart disease. *Eur. Heart J.*, **14**, 150-159.

Van der Hoeven, G.W.G., Clerens, P.J.A., Donders, J.J.H., Beneken, J.E.W. & Vonk, J.T.C. (1977) A study of systolic time intervals during uninterrupted exercise. *Br. Heart J.*, **39**, 242-254.

Vanfraechem, J.H.P. (1979) Stroke volume and systolic time interval adjustments during bicycle exercise. *J. Appl. Physiol.*, **46**, 588-592.

Vanhees, L., Fagard, R., Grauwels, R., Wijhoven, J., De Geest, H. & Amery, A. (1984) Systolic time intervals in coronary heart disease at rest and during exercise: Effect of physical training with and without beta blockade. *Am. J. Cardiol.*, **54**, 508-513.

Wang, X., Sun, H.H. & Van de Water, J.M. (1995) Time-frequency distribution technique in biological signal processing. *Biomed. Instrum. Technol.*, **29**, 203-212.

Wolfe, L.A., Cunningham, D.A., Davis, G.M. & Rechnitzer, P.A. (1978) Reliability of noninvasive methods for measuring cardiac function in exercise. *J. Appl. Physiol.*, **44**, 55-58.

Attenuated Respiratory Modulation of Chemoreflex-Mediated Sympathoexcitation in Patients With Chronic Heart Failure

HIROSHI UENO, MD, HIDETSUGU ASANOI, MD, KUNIHIRO YAMADA, MD, YOSHITAKA ODA, MD, JUNYA TAKAGAWA, MD, TOMOKI KAMEYAMA, MD, TADAKAZU HIRAI, MD, TAKASHI NOZAWA, MD, SHUTARO TAKASHIMA, MD, AND HIROSHI INOUE, MD

Toyama, Japan

ABSTRACT

Background: Enhanced hypercapnic chemoreflex in chronic heart failure could modulate sympathetic nerve activity in a different manner depending on the severity of heart failure. This study was designed to evaluate the dynamic aspects of sympathoexcitation caused by central hypercapnic chemoreflex in patients with chronic heart failure.

Methods and Results: In 21 patients with chronic heart failure, wavelet analysis was applied to elucidate the spectral components of muscle sympathetic nerve activity (MSNA) and instantaneous ventilation during hypercapnic chemoreceptor stimulation. Hypercapnia increased MSNA (83 ± 8 versus 29 ± 9 %, $P < .01$) and ventilation (209 ± 27 versus 190 ± 21%, $P < .05$) more in 12 symptomatic patients than in 9 asymptomatic patients. This hypercapnic chemoreflex exerted a greater influence on the sympathetic limb than on the ventilatory limb in the symptomatic patients. The wavelet analysis revealed that the within-breath sympathoinhibition in the symptomatic patients was attenuated as compared with that in the asymptomatic patients (0.33 ± 0.03 vs. 0.44 ± 0.04, $P < .05$).

Conclusions: The enhanced chemoreflex sympathetic drive and relative attenuation of ventilatory sympathoinhibition could contribute to exaggerated sympathoexcitation in patients with heart failure when they are exposed to carbon dioxide during exercise or sleep apnea.

Key Words: Muscle sympathetic nerve activity, central chemoreflex, lung stretch reflex, wavelet analysis.

Heart failure is characterized by sympathetic overactivation that contributes a great deal to progression and prognosis of this disorder. Recently, sympathoexcitatory reflexes have started to receive considerable attention as potential mechanisms for the heightened sympathetic drive.[1-5] One of the major excitatory reflexes originates from peripheral and central chemoreceptors. Recently several investigators[1,5] have shown the augmentation of central chemoreflex sensitivity underlies excessive exercise ventilation in patients with chronic heart failure. Although the chemoreflex also elicits sympathetic activation, the concomitant increase in lung inflation activates pulmonary vagal afferents that reflexively inhibit sympathetic nerve discharge.[3,6-8] These 2 opposing mechanisms, which would depend upon physiologic state, determine the net effect of the chemoreflex on sympathetic nerve activity. We have previously demonstrated in patients with heart failure that suppression of muscle sympathetic nerve activity (MSNA) by the lung stretch reflex was attenuated in patients with severe heart failure.[3] Under these conditions, we hypothesized that hypercapnic chemoreflex could result in a greater sympathetic drive as the heart failure progresses.

The purpose of the present study was, therefore, to compare sympathetic and ventilatory responses with hypercapnic chemoreceptor activation and to evaluate respiratory modulation of chemoreflex control of sympathetic nerve activity in patients with chronic heart failure. To quantify the dynamic nature of respiratory modulation of chemoreflex-mediated sympathoexcitation, we applied wavelet analysis for a progressive augmentation in MSNA and ventilation during hypercapnia.[9]

From the Second Department of Internal Medicine, Toyama Medical and Pharmaceutical University, Toyama, Japan

Manuscript received June 5, 2003; revised manuscript received September 4, 2003; revised manuscript accepted September 30, 2003.

Reprint requests: Hidetsugu Asanoi, MD, The Second Department of Internal Medicine, Toyama Medical and Pharmaceutical University, 2630 Sugitani, Toyama 930-0194, Japan.

Supported by Grant-in-Aid for General Scientific Research No 13670697 from the Ministry of Education, Science and Culture of Japan.

1071-9164/$ - see front matter

doi:10.1016/j.cardfail.2003.09.005

Methods

Study Patients

The present study included 21 patients with stable heart failure (18 men and 3 women) with left ventricular ejection fraction <45 % determined by radionuclide or contrast ventriculography (Table 1). Each patient's quality of life was quantified by a specific activity scale (SAS) on questionnaires for ordinary physical activities.[10] Subjects were prospectively divided into 2 groups: 9 asymptomatic patients (New York Heart Association class I) and 12 symptomatic patients (class II: 5; class III: 7). Fourteen patients had dilated cardiomyopathy, 3 had previous myocardial infarction, and 4 had regurgitant valvular heart disease. Nine patients were in atrial fibrillation. Patients with lung disorders, anemia, severe hypoxemia (partial pressure of arterial oxygen <80 mm Hg), diabetes mellitus, or autonomic failure of other origins were excluded from the present study. Concurrent medications included angiotensin-converting enzyme inhibitors in 14 patients, digitalis in 9, and diuretics in 15. None of the subjects had β-blockers and a history of more than occasional alcohol consumption. Informed written consent was obtained from all patients. The study was approved by the Institutional Human Subjects Review Committee.

Measurements

All measurements were performed with subjects in resting supine conditions, as reported previously.[11] Blood pressure was serially recorded with noninvasive tonometry (Jentow 7700, Colin, Komaki, Japan). Respiratory flow was measured continuously on a breath-by-breath basis with the thermal dissipation technique (AE-280, Minato, Osaka, Japan). Multiunit recording of efferent postganglionic sympathetic nerve activity to the skeletal muscle district was obtained with a microelectrode inserted directly into the left peroneal nerve posterior to the fibular head. The nerve signal was amplified by 100,000, fed through a band-pass filter (500 to 5000 Hz), and integrated with a custom nerve-traffic analysis system (NeuropackΣ MEB-5504, Nihonkoden, Tokyo, Japan). Integrated nerve activity together with analog blood pressure tracing, electrocardiogram, and respiratory flow were digitized at 1000 Hz per channel by an analog-digital converter (DT9804-USB, Data Translation Inc., Marlboro, Massachusetts) and directly stored on a hard-disk memory system (DynaBook Satellite 2270, Toshiba, Tokyo, Japan). To evaluate baseline cardiac function, chest radiograph, radionuclide or contrast ventriculography, and arterial blood gas were measured in all patients. Blood samples were drawn from the antecubital vein with the subject at rest for measurements of plasma concentrations of norepinephrine and brain natriuretic peptide.

Table 1. Patient Characteristics

	Asymptomatic (NYHA I: 9)	Symptomatic (NYHA II + III: 12)	*P*
Age (y)	55 ± 5	62 ± 3	NS
Sex (male/female)	8/1	10/2	NS
Body weight (kg)	68 ± 3	58 ± 3	NS
SAS (METs)	7.2 ± 0.1	3.9 ± 0.4	<.01
CTR (%)	54 ± 15	60 ± 18	<.05
LVEF (%)	35 ± 11	36 ± 9	NS
NE (pg/mL)	284 ± 5	490 ± 55	<.05
BNP (pg/mL)	60 ± 15	280 ± 69	<.01
ABG			
pH	7.42 ± 0.01	7.40 ± 0.04	NS
PaO_2 (mm Hg)	89 ± 3	91 ± 3	NS
$PaCO_2$ (mm Hg)	41 ± 1	38 ± 1	<.05
Etiology			
DCM	7	7	
OMI	1	2	
VHD	1	3	
Concurrent medication			
ACEI	6	8	
Digitalis	3	6	
Diuretics	3	9	

Values are mean ± standard error of the mean.

NYHA, New York Heart Association; NS, not significant; SAS, specific activity scale; CTR, cardiothoracic ratio; LVEF, left ventricular ejection fraction; NE, plasma norepinephrine; BNP, brain natriuretic peptide; ABG, arterial blood gas analysis; PaO_2, arterial partial pressure of oxygen; $PaCO_2$, arterial partial pressure of carbon dioxide; DCM, dilated cardiomyopathy; OMI, old myocardial infarction; VHD, regurgitant valvular heart disease; ACEI, angiotensin-converting enzyme inhibitor.

Study Protocol and Data Analysis

Baseline recordings of electrocardiogram, blood pressure, respiratory flow, and MSNA were performed for 3 minutes while patients were breathing room air in the supine position. Then, subjects rebreathed a hyperoxic hypercapnic gas mixture (7% carbon dioxide [CO_2] and 93% oxygen [O_2]) for 4 minutes to activate central hypercapnic chemoreflex while peripheral chemoreflex was suppressed by hyperoxia. Systolic and diastolic pressures were determined from each beat of the arterial pressure signals. Instantaneous ventilatory volume was calculated from the integration of respiratory flow. Tidal volume was calculated from the peak of instantaneous ventilatory volume in each breath. Instantaneous ventilatory volume, MSNA, and blood pressure were splined and resampled at 4 Hz. Sympathetic neural bursts were identified by careful inspection of the voltage neurogram. The amplitude of each burst was determined, and sympathetic activity was calculated as bursts per 100 heartbeats. To evaluate quantitative changes in sympathetic nerve activity in each individual, the area of sympathetic neural bursts was measured after subtraction of the baseline drift of MSNA and the burst amplitude was expressed as the percentage of the maximal baseline value. The dynamic increases in sympathetic tone and ventilation were analyzed by the spectral estimation based on the discrete wavelet transform using Gabor basis wavelet, as described previously.[9,12] This method has a great advantage over the traditional stationary spectral analysis in that the wavelet distribution could provide beat-to-beat spectral analysis and illustrate transitional spectral changes within the 3-dimensional framework of power, time, and frequency. The frequency contents were divided into respiratory components (0.15–0.5 Hz) and pulse-synchronous components (0.51–2.0 Hz). We also applied the wavelet analysis for diastolic blood pressure during chemoreflex activation to quantify the respiratory components (0.15–0.5 Hz) of diastolic blood pressure variability.

Statistical Analysis

Data are expressed as mean ± standard error of the mean. Baseline characteristics between the 2 groups were compared by unpaired *t*-test. Responses to hypercapnia between asymptomatic and symptomatic patients were compared with analysis of variance for repeated measures followed by Bonferroni's method for multiple comparisons. Analyses were performed using statistical software (Sigma Stat version 2.03, SPSS Inc., Chicago, Illinois). The level of statistical significance was set at $P < .05$.

Results

Effects of Hypercapnia

Clinical and hemodynamic features of the subjects are shown in Table 1. The groups were comparable for age, body weight, and distribution of the etiology of cardiac dysfunction. Similarly, there were no significant differences in the resting left ventricular ejection fraction, heart rate, and blood pressure between the 2 groups. However, the symptomatic patients had a lower physical activity assessed by SAS and a larger cardiothoracic ratio compared with the asymptomatic patients. Although there were no significant differences in arterial O_2 partial pressure, the symptomatic patients had a significantly lower arterial CO_2 partial pressure. The baseline sympathetic tone was greater in the symptomatic patients as reflected by a significant increase in plasma norepinephrine levels.

The influences of hypercapnia are summarized in Table 2 and Fig. 1. The baseline respiratory rate, tidal volume, and minute ventilation were comparable in both groups. Although hypercapnia elicited a comparable increase in heart rate and blood pressure, there were substantial differences in ventilatory and sympathetic responses to hypercapnia between the 2 groups. Hypercapnic chemoreflex activation increased both minute ventilation and MSNA more in the symptomatic patients than in the asymptomatic patients. Furthermore, the relative increase in MSNA for a given increase in ventilation was also greater in the symptomatic patients than in the asymptomatic patients. Tidal volume during hypercapnia was comparable between the 2 groups, where an increase in respiratory rate contributed a lot to a greater increase in minute ventilation in the symptomatic patients. Although cardiac function assessed by left ventricular ejection fraction and plasma brain natriuretic peptide did not correlated with changes in MSNA, there was a significant inverse correlation between the baseline SAS and the increase in MSNA burst area during hypercapnia ($r = -.47$, $P < .05$).

Table 2. Effects of Hypercapnia (Maximum Response)

	Asymptomatic (n = 9)	Symptomatic (n = 12)	*P*
HR (beats/min)			
Control	72 ± 4	68 ± 4	NS
Hypercapnia	80 ± 5*	82 ± 5*	NS
MBP (mm Hg)			
Control	82 ± 3	78 ± 4	NS
Hypercapnia	96 ± 4*	88 ± 6*	NS
RR (breaths/min)			
Control	16 ± 1.5	16 ± 0.8	NS
Hypercapnia	18 ± 1.6	22 ± 1.7*	NS
TV (mL/m^2)			
Control	309 ± 26	381 ± 29	NS
Hypercapnia	763 ± 69*	843 ± 68*	NS
VE (L/min/m^2)			
Control	4.8 ± 0.6	5.8 ± 0.4	NS
Hypercapnia	13.7 ± 1.5*	18.1 ± 1.8*	<.05
MSNA burst area (×10^3%/min)			
Control	1069 ± 90	1110 ± 80	NS
Hypercapnia	1360 ± 121*	2021 ± 171*	<.05
ΔMSNA area/ΔVE (×10^3·m^2/L)	28.1 ± 7.7	85.4 ± 12.1	<.05

*$P < .05$.

Values are mean ± standard error of the mean.

HR, heart rate; MBP, mean blood pressure; MSNA, muscle sympathetic nerve activity; RR, respiratory rate; TV, tidal volume; VE, minute ventilation.

Instantaneous Spectral Power of MSNA and Ventilation

Spectral components obtained from wavelet analysis are shown in Table 3. Although hypercapnia increased respiratory fluctuations of diastolic blood pressure, there was no significant difference in the magnitude between asymptomatic and symptomatic patients. The dynamics of MSNA burst fluctuation and ventilation during hypercapnia are shown within the time-varying spectral framework in Fig. 2. The continuous spectral plots of ventilation demonstrated that the instantaneous ventilatory power rose gradually in both groups with a shift toward higher frequencies (increase in respiratory rate) as CO_2 rebreathing time elapsed. Within the spectral plots of MSNA, respiratory components of MSNA power (0.15–0.5 Hz) were manifested with an increase in instantaneous ventilation in the asymptomatic patients, whereas pulse-synchronous components (0.51–2.0 Hz) remained unchanged. In the symptomatic subjects, however, the pulse-synchronous components of MSNA power rose progressively and predominated over the respiratory components during CO_2 rebreathing.

When plotted against the instantaneous ventilatory power (Fig. 3), pulse-synchronous spectral components of MSNA rose with a similar slope in both groups up to 1 minute of CO_2 rebreathing. In the symptomatic patients, these components of MSNA progressively rose up to the late phase (>1 minute) while reaching a plateau in the asymptomatic patients. In contrast, the relative magnitude of respiratory components of MSNA power as reflected by the ratio to the total power fell in the symptomatic patients, whereas it rose significantly in the asymptomatic patients ($P < .05$ for group-by-time interaction). There was a significant inverse correlation between the increase in total MSNA area and the changes in the ratio of respiratory components to the total MSNA power ($r = .49$, $P < .05$) in all patients.

Discussion

The present study compared relative magnitude of pulse-synchronous components of MSNA power with that of within-breath suppression of MSNA during hypercapnic chemoreflex activations using the wavelet analysis in patients with heart failure. As the heart failure progressed, hypercapnic chemoreflex influenced the sympathetic limb more profoundly than the ventilatory limb. Consequently, in the symptomatic patients, the respiratory suppression of

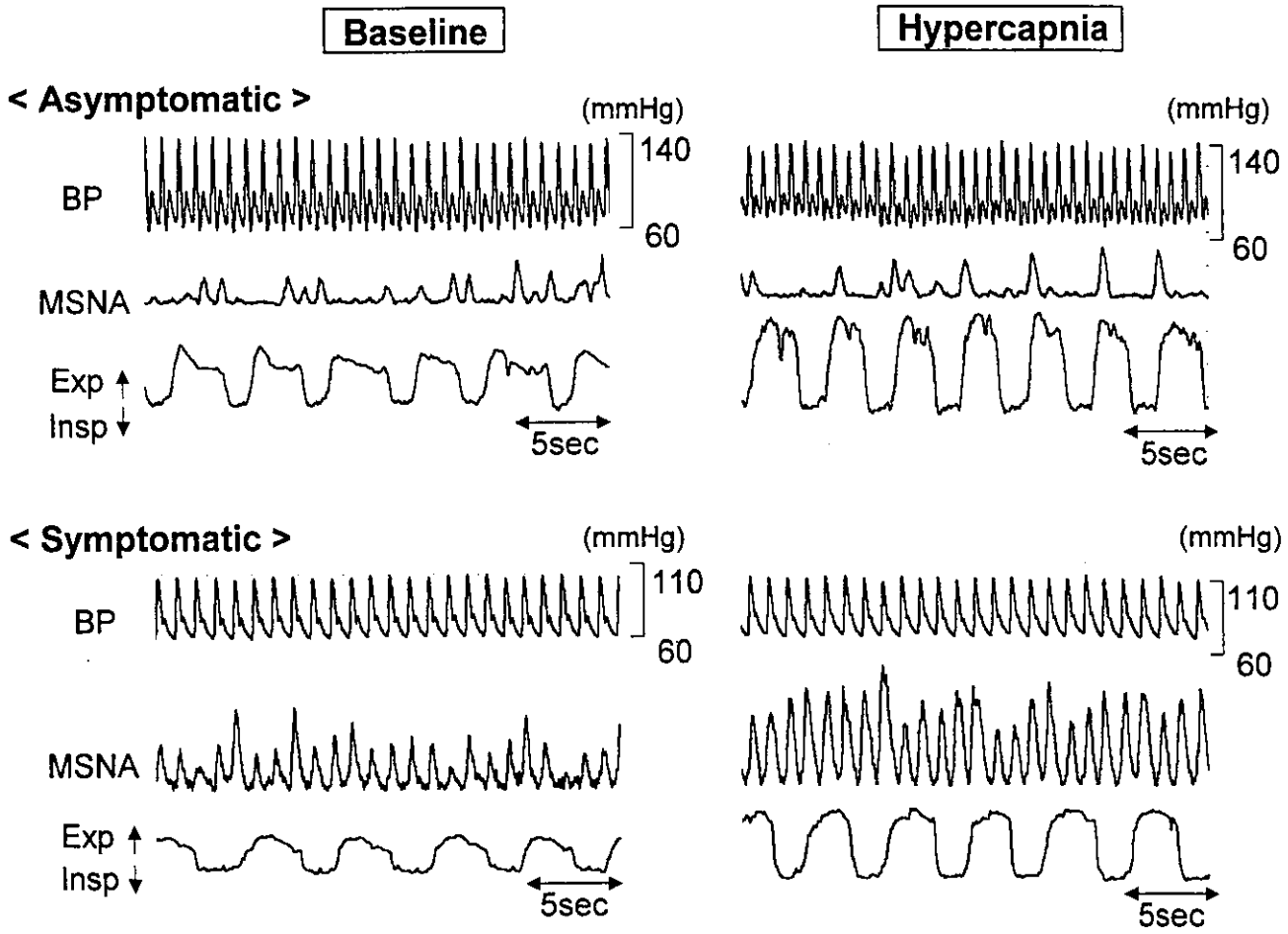

Fig. 1. Blood pressure (BP) tracings, muscle sympathetic nerve activity (MSNA), and respiratory flow curves at baseline and during hypercapnia over 2 minutes in an asymptomatic patient (top) and a symptomatic patient (bottom). In the symptomatic patient, hypercapnia induced greater increase in MSNA with no neural silence caused by respiration. Exp, expiration; Insp, inspiration.

MSNA was overridden by a substantial increase in the pulse-synchronous bursts. In the asymptomatic patients, however, chemoreflex-induced hyperventilation was accompanied by dominant inspiratory suppression of MSNA during hypercapnia. These findings suggest that, in patients with advanced heart failure, sympathoexcitatory mechanisms through hypercapnic chemoreflex predominated over the sympathoinhibitory counteraction of lung stretch reflex.

Enhanced Sympathetic and Ventilatory Chemoreflexes

Recently, several sympathoexcitatory mechanisms, including peripheral and central chemoreflexes and cardiac sympathetic afferents, received special attention.[5,9,12,13] Enhanced ventilatory response to hypercapnic chemoreflex activation has been well documented in heart failure.[1,14] The study by Narkiewics et al.[5] was the first that demonstrated an enhanced sympathetic response to hypercapnic chemoreflex activation in heart failure. Our data are concordant with their findings. The present study also clarified sympathetic and ventilatory interaction on beat-by-beat and breath-by-breath basis during hypercapnic chemoreflex activation in patients with different functional capacity. The increase in sympathetic nerve activity is reflected as an increase in burst frequency and amplitude of MSNA, which are entrained to cardiac cycle. Over the breath cycle, lung inflation also exerts a rhythmic inhibitory influence on central sympathetic outflow.[3,6–8] Somers et al.[15] have shown that cessation of breathing during hypercapnia had a tonic influence on sympathetic nerve activity. We have previously demonstrated that, in patients with heart failure, sympathetic activity is closely coupled with respiration on a breath-by-breath basis and suppressed more effectively by greater lung inflation with fixed delay time of 1.5 seconds.[3] The wavelet analysis employed in the present study is capable of separating pulse-synchronous and respiratory fluctuations of MSNA and revealing the dynamic nature of their serial changes during hypercapnia. Within 1 minute of hypercapnia, all spectral components of MSNA showed a parallel increase with instantaneous ventilatory volume in both groups, whereas the magnitude of these responses was greater in the symptomatic patients. After one minute of CO_2 exposure, the symptomatic patients demonstrated a greater sympathetic response